VERTICAL STRUCTURE OF THE UNDERTOW OUTSIDE THE SURF-ZONE

UDAY PUTREVU and IB A. SVENDSEN

RESEARCH REPORT NO. CACR-94-09

February 1994

CENTER FOR APPLIED COASTAL RESEARCH

Ocean Engineering Laboratory
University of Delaware
Newark, Delaware 19716

Vertical Structure of the Undertow Outside the Surf-Zone

Uday Putrevu and Ib A. Svendsen

Center for Applied Coastal Research, Department of Civil Engineering

University of Delaware, Newark, DE 19716

Abstract

The vertical structure of the undertow in the shoaling region outside the surf-zone is quite different from that inside the surf-zone. Inside the surf-zone the undertow typically has a large seaward directed velocity near the bottom and either a shoreward directed or a small seaward directed velocity at trough level. Measurements show that outside the surf-zone the undertow has a small seaward directed velocity near the bed and a large seaward directed velocity at trough level. In this note we develop theoretical expressions for the undertow outside the surf-zone and show that the steady streaming from the bottom boundary layer which was earlier found to have a negligible effect in the surf-zone (Svendsen *et al.* 1987) does have a significant influence on the vertical structure of the undertow in that region.

1 Introduction

Consider waves normally incident on a beach so that at any point there is no net cross-shore flow. A seaward directed return flow, the undertow, is then generated below trough level

to compensate for the wave induced volume flux above that level. The mechanisms responsible for the undertow were discussed by Dyhr-Nielsen & Sorenson (1970) and analyzed by Svendsen (1984), Dally & Dean (1984), Stive & Wind (1986), Svendsen *et al.* (1987), Svendsen & Hansen (1988) and Okayasu *et al.* (1988). Detailed laboratory measurements of the undertow include Stive & Wind (1982), Nadaoka & Kondoh (1982), Hansen & Svendsen (1984, 1986), Okayasu *et al.* (1986, 1988) and Ting & Kirby (1993). Field measurements include Wright *et al.* (1982), Guza & Thornton (1985) and Greenwood & Osborne (1990). However, the models for the calculation of undertow have so far only been applied to calculate the undertow inside the surf-zone. No effort seems to have been made to calculate the undertow in the shoaling region outside the surf-zone although the relatively few measurements available in that region suggest that there are significant differences, which may signify differences, at least in the importance of the different mechanisms involved, relative to what has been found inside the surf-zone.

Figure 1 (from Nadaoka & Kondoh 1982) shows a measured variation of the undertow with cross-shore location. Inside the surf-zone, the dominant feature is that the undertow profiles show rather strong seaward flows near the bed ($U_b/\sqrt{gh} \sim 0.1$ where U_b is the bottom velocity and h is the local water depth) and either a shoreward flow or a weak seaward flow at trough level. Svendsen *et al.* (1987; referred to hereafter as SSH) showed that the presence of a wave boundary layer with a much lower level of turbulence than the rest of the water column can explain the large seaward oriented bottom velocities inside the surf-zone. In the region between the bottom and the wave trough level the major driving force was found to be the pressure gradient from the slope on the mean water level (set up) whereas the opposing radiation stress contribution was much smaller. They also analyzed the effect of the steady streaming and found it to have a negligible effect on the undertow profile.

Outside the surf-zone, the undertow shows remarkably different features. First, the undertow profile has very little curvature and, second, it typically has a small seaward directed velocity at the bed and a large seaward oriented velocity at trough level. These features appear in all undertow measurements outside the surf-zone (Nadaoka & Kondoh

1982; Hansen & Svendsen 1984, 1986; Okayasu *et al.* 1986, 1988; Hwung & Lin 1990; Ting & Kirby 1993). The aim of the present note is to illustrate the mechanisms responsible for this behavior. Though elements of the undertow model turn out to be very similar to the one developed by Svendsen & Hansen (1988), the actual mechanisms are quite different due to the absence of wave breaking.

The theoretical analysis is presented in section 2. The numerical results for the undertow profiles are presented in section 3 where we analyze the mechanism responsible for the shape of the undertow profiles outside the surf-zone. In that section the model results are also compared with available experimental data. The paper concludes with a discussion in section 4.

2 Mathematical Formulation (Model)

The equation governing the undertow is the wave averaged cross-shore momentum equation. For simplicity, we limit the discussion to the case of long waves ($\overline{w_w^2} \ll \overline{u_w^2}$ where w_w and u_w refer to the wave induced vertical and horizontal velocities respectively). The wave averaged cross-shore momentum equation may then be written as (see, *e.g.,* Svendsen & Lorenz 1989)

$$-\frac{\partial}{\partial z}\left(\overline{u'w'}\right) = g\frac{d\bar{\zeta}}{dx} + \overline{\frac{\partial u_w^2}{\partial x}} + \overline{\frac{\partial u_w w_w}{\partial z}} \tag{1}$$

The geometrical quantities used in the above are defined in figure 1. In the case of long waves ($\partial u_w/\partial z = 0$) this may, outside the bottom boundary layer, be written as

$$-\frac{\partial}{\partial z}\left(\overline{u'w'}\right) = g\frac{d\bar{\zeta}}{dx} + \frac{1}{2}\overline{\frac{\partial u_w^2}{\partial x}} = \alpha_1(x) \tag{2}$$

In most previous analyses the $\partial/\partial z$ term has been neglected on the ground that for a symmetrical wave like a sine wave $\overline{u_w w_w} = 0$. Inside the surf-zone this is of little consequence because the $\overline{u_w^2}$ and $\overline{u_w w_w}$ terms are small relative to the $g\bar{\zeta}$ term.

Outside the surf-zone, however, it turns out that the situation is different in that the $\overline{u_w^2}$ term is of the same order of magnitude as the $g\bar{\zeta}$ term. It then becomes important

that since the waves are shoaling they are not purely symmetrical, so $\overline{u_w w_w} \neq 0$. In fact, it can be argued that if the waves were symmetrical so that $\overline{u_w w_w} = 0$ we would also have $\partial \overline{u_w^2}/\partial x = 0$ so that both the second and third terms on the RHS of (1) would vanish, and so would the first.

The assumption $\partial u_w/\partial z = 0$, on the other hand, is valid even for non-symmetrical, finite amplitude long waves. Thus we use (2) to determine the undertow. It is interesting to note that the the contribution to $\overline{u_w w_w}$ originating from the bottom boundary condition $w_w = -u_w h_x$ does not enter the equation because it has $\partial/\partial z = 0$ in this approximation.

Introducing an eddy viscosity closure to model the correlation of the turbulent fluctuations then leads to

$$\frac{\partial}{\partial z}\left(\nu_{tz}\frac{\partial U}{\partial z}\right) = \alpha_1(x) \tag{3}$$

which has the solution

$$U(x,z) = \alpha_1 \int_{-h_0}^{z} \frac{1}{\nu_{tz}} \int_{-h_0}^{z} dz dz + C_1 \int_{-h_0}^{z} \frac{1}{\nu_{tz}} dz + U_b \tag{4}$$

where C_1 and U_b are integration constants, the latter being the bottom velocity.

Determination of C_1 and U_b follows the arguments given by Svendsen & Hansen (1988) and the following is a condensed version of the solution. We assume the existence of a (thin) bottom boundary layer with a significantly lower level of turbulence than the rest of the water column (SSH). We model the flow field by assuming that the water column may be split into two layers – the bottom boundary layer and the upper layer above. For simplicity, we also assume depth uniform eddy viscosities in these two regions.

Inside the bottom boundary layer the eddy viscosity is denoted by ν_{tg} and the equation governing the undertow may be written in the following form

$$\frac{\partial}{\partial z}\left(\nu_{tg}\frac{\partial U}{\partial z}\right) = g\frac{d\bar{\zeta}}{dx} + \overline{\frac{\partial u_w^2}{\partial x}} + \overline{\frac{\partial u_w w_w}{\partial z}} \tag{5}$$

Since the eddy viscosity used is discontinuous at the top of the boundary layer the solutions to equations 3 and 5 are matched at that level using continuity in velocity U and

the shear stress $\nu_t(\partial U/\partial z)$. The constants U_b and C_1 in (4) are then determined by two boundary conditions. The first is obtained by integrating (5) from the bed $z = -h_0$ to the top of the boundary layer $z = -h_0 + \delta$ which leads to

$$\nu_{tg}\frac{\partial U}{\partial z}\Big)_{z=-h_0+\delta} - \frac{\tau_b}{\rho} = \overline{u_w w_w}\big)_{z=-h_0+\delta} + \int_{-h_0}^{-h_0+\delta}\left(g\frac{d\bar{\zeta}}{dx} + \overline{\frac{\partial u_w^2}{\partial x}}\right)dz \tag{6}$$

where we have used the fact that $\rho\nu_{tg}(\partial U/\partial z)_{z=-h_0} = \tau_b$, the bottom shear stress.

The first term on the RHS of (6) is related to the steady streaming in the bottom boundary layer and the second term essentially represents the curvature of the undertow inside the bottom boundary layer. The results of SSH show that this term is small and, therefore, we neglect it here.

Introducing the notation

$$\tau_{sb} = -\rho\overline{u_w w_w}\big)_{z=-h_0+\delta} \tag{7}$$

we get

$$\nu_{tg}\frac{\partial U}{\partial z}\Big)_{z=-h_0+\delta} \approx \frac{\tau_b}{\rho} - \frac{\tau_{sb}}{\rho} \tag{8}$$

which by virtue of the matching conditions becomes the first boundary condition for the undertow in the upper layer, *viz.*,

$$\nu_{tz}\frac{\partial U}{\partial z}\Big)_{z=-h_0} = \nu_{tg}\frac{\partial U}{\partial z}\Big)_{z=-h_0+\delta} = \frac{\tau_b}{\rho} - \frac{\tau_{sb}}{\rho} \tag{9}$$

The second boundary condition is given by the constraint of no net cross-shore flow which leads to

$$\int_{-h_0}^{\bar{\zeta}} U dz = -Q_w \tag{10}$$

where Q_w is the volume flux due to the wave motion defined by

$$Q_w = \overline{\int_{-h_0}^{\zeta} u_w dz} = \overline{\int_{\zeta_t}^{\zeta} u_w dz} \tag{11}$$

The second part of (11) follows from the fact that we have $\overline{u_w} = 0$ below trough level ($z = \zeta_t$). Equation 10 involves the definition of the current above trough level and may deserve some explanation.

Below trough level, decomposing the water motion into a current part and a wave induced part is relatively straightforward – the current is defined as the component of the velocity that remains after averaging over a wave period. Above trough level there is water only part of the time and such an operation is not straightforward. To get around this problem, while still operating in the wave averaged domain, two approaches have been taken in the literature. The first of these defines a current only below trough level – it assumes the entire motion above that level to be a part of the wave motion. In this approach the u_w in (11) would then represent the total water motion above trough level. This approach has been used by Hansen & Svendsen (1984), Stive & Wind (1986), deVriend & Stive (1987), SSH, Stive & deVriend (1987) and Svendsen & Hansen (1988). The alternative approach used consists of decomposing the water motion into a current part and a wave induced part and clearly specifying how a current is defined above trough level. Investigators that have used this approach typically assume that the mathematical expression that defines the current below trough level is valid above that level also – Phillips (1977) and Mei (1983) for depth uniform flow and Svendsen & Hansen (1986) and Svendsen & Putrevu (1993) for non-uniform flow.

Though the net result of the two approaches will be the same we have decided to adopt the second approach here since we have found elsewhere (Svendsen & Putrevu 1993) that the calculation of the dispersion effect caused by the interaction of nearshore currents becomes much simpler if we follow this approach.

With a depth uniform eddy viscosity ν_{tz} and determining C_1 from (9), (4) yields

$$U(x,z) = \frac{\alpha_1}{2\nu_{tz}}(z+h_0)^2 + \frac{\tau_b - \tau_{sb}}{\rho\nu_{tz}}(z+h_0) + U_b \tag{12}$$

Finally, we assume that the bed shear stress is related to the near bottom velocity U_b by

$$\tau_b = \frac{2}{\pi}\rho f_w u_{wb} U_b \tag{13}$$

where f_w is a friction factor and u_{wb} is the amplitude of the near bottom wave induced

velocity, and the steady streaming term is given by the value for linear long waves, *viz.*,

$$\tau_{sb} = \frac{-1}{2}\rho\nu_{tg}\beta\frac{u_{wb}^2}{c} \tag{14}$$

(see, e.g., Phillips 1977, p. 55). In the above c is the wave celerity and

$$\beta = \sqrt{\frac{\omega}{2\nu_{tg}}} \tag{15}$$

where ω is the wave frequency ($= 2\pi/T$, T being the wave period).

Once the parameters ν_{tg}, ν_{tz} and α_1 are specified, the undertow is readily determined by solving for U_b from (10). This leads to

$$\frac{U_b}{\sqrt{gh}} = \left(\frac{U_m}{\sqrt{gh}} - \frac{A}{6} + \frac{\overline{\tau_{sb}}h}{2\rho\nu_{tz}\sqrt{gh}}\right)(1+R_1)^{-1} \tag{16}$$

where

$$A = \frac{\alpha_1 h^2}{\nu_{tz}\sqrt{gh}} \tag{17}$$

$$R_1 = \frac{f_w u_{wb} h}{\pi\nu_{tz}} \tag{18}$$

and

$$U_m = \frac{-Q_w}{h} \tag{19}$$

The result given by (12) is valid both inside and outside the surf-zone. The differences in the solutions inside and outside the surf-zone come from the differences in the variations of α_1, ν_{tg} and ν_{tz} in those regions. In the next section, numerical results are presented and compared with experiments.

3 Numerical Results

3.1 Parameter Values

Inside the surf-zone the slope on the mean water level dominates the RHS of (2). SSH found

$$\alpha_1 = 0.1gh_x \tag{20}$$

to be a reasonable approximation of the forcing inside the surf-zone. Outside the surf-zone the slope on the mean water level is much smaller than it is inside the surf-zone. Hence, we expect that both terms on the RHS of (2) will be important. Linear long wave theory has

$$S_{xx} = \frac{3}{16}\rho g H^2 \tag{21}$$

$$u_w = c\frac{\eta}{h} = c\frac{H}{2h}\cos\omega t \tag{22}$$

which means

$$\overline{u_w^2} = c^2\frac{H^2}{8h^2} \tag{23}$$

The slope on the mean water level is determined by the depth integrated horizontal momentum equation

$$g\frac{d\bar{\zeta}}{dx} = \frac{-1}{\rho h}\frac{dS_{xx}}{dx} - \frac{\tau_b}{\rho h} \tag{24}$$

Using the above (and the fact that $H \propto h^{-1/4}$ for linear long waves) we find that, outside the surf-zone,

$$\alpha_1 = g\frac{d\bar{\zeta}}{dx} + \overline{u_w\frac{du_w}{dx}} = -\frac{\tau_b}{\rho h} \tag{25}$$

where τ_b is given by (13).

Inside the surf-zone SSH also found

$$\nu_{tz} \sim 0.01h\sqrt{gh} \tag{26}$$

The variation of this parameter is not known outside the surf-zone. However, we may estimate the variation using qualitative arguments and the turbulence measurements of Nadaoka & Kondoh (1982) as a guide. These measurements are reproduced in figure 3. They show that there is in fact a significant level of turbulence outside the surf-zone. The detailed variation of ν_{tz} with h is less important, so we assume, in keeping with the measurements, that

$$\nu_{tz} = \left[0.2 + 0.8\left(\frac{h_b}{h}\right)^4\right]\nu_{tzb} \tag{27}$$

where ν_{tzb} is the eddy viscosity at breaking.

The eddy viscosity in the bottom boundary layer is related to the turbulence level inside the bottom boundary layer and is expected to vary as H/h and based on careful measurements in the literature (see SSH for discussion) is taken to be (using $f_w = 0.02$)

$$\frac{\nu_{tg}}{h\sqrt{gh}} = 0.08 f_w^2 \left(\frac{H}{h}\right)^2 \sim 3 \times 10^{-5} \left(\frac{H}{h}\right)^2 \tag{28}$$

As will be demonstrated below, the exact value of ν_{tg} is unimportant for the main features of the results. However, the estimate does suggest that ν_{tg} decays much slower in the seaward direction than ν_{tz} as one would expect from the physics of the problem.

3.2 Results

Figure 4 shows the undertow profiles calculated neglecting the steady streaming. The additional parameters used in this figure are $H/h = 0.7$ (inside the surf-zone), $Q_w = 0.06(H^2/h)\sqrt{gh}$, $h_b = 20cm$, $T = 3s$ and $h_x = 1/30$. The single strongly varying curve in this figure represents the undertow profiles inside the surf-zone which for the simplifications made are the same at all locations. The other curves represent undertow profiles at various locations outside the surf-zone. A comparison of the shape of the profiles in figure 4 with the measurements shown in figure 1 shows that while the calculated profiles inside the surf-zone are reasonable the general characteristics of the calculated profiles outside the surf-zone are quite different from what the measurements show.

In contrast, figure 5 shows the undertow profiles calculated including the steady streaming. The other parameters used in this calculation are the same as those used in the calculations for figure 4. Therefore, a comparison of the two figures shows the effect of the steady streaming on the solution. Such a comparison clearly confirms SSH's earlier result that the steady streaming has very little influence on the undertow inside the surf-zone. Outside the surf-zone, however, the effect is very substantial and is essentially responsible for the different shape of the profiles.

Equations 12 and 14 indicate that the effect of the steady streaming increases with the ratio ν_{tg}/ν_{tz}. However, our estimates of this ratio are quite uncertain. To analyze the

sensitivity of the velocity profiles to this uncertainty, figures 6 and 7 show the variation of the undertow profiles for two very different values of ν_{tg}/ν_{tz} (100, 1000 respectively) with ν_{tz} given by (26) and (27). These values span the expected range of variation for the ratio ν_{tg}/ν_{tz}. Figures 5, 6 and 7 demonstrate that within a wide range of values of ν_{tg}/ν_{tz} the general trend of the results in figure 5 is unaffected by the precise value of that ratio.

3.3 Comparison with Experimental Data

We have also compared the model predictions for the undertow outside the surf-zone with available experimental data. The data comes from the experiments of of Nadaoka & Kondoh (1982, denoted by N & K), Hansen & Svendsen (1984, denoted by H & S) and Ting & Kirby (1993, denoted by T & K). Since figure 3 shows that the turbulence level outside the breaking point depends somewhat on the type of breaking we have divided the comparison between spilling and plunging breaker cases.

Figure 8 shows the model predictions together with the experimental data for spilling breakers. In the computations ν_{tz} is taken to be $0.008h\sqrt{gh}$ inside surf-zone and (27) outside. The parameters f_w, Q_w and ν_{tg} are as in the example presented in the previous section. The values of H/h, T and h_x are taken from the experiments. The figure demonstrates that the model results are quite close to the experimental data. Given the uncertainty associated with the estimation of some parameters and the use of linear wave theory so close to breaking, the agreement is actually remarkable.

Figure 9 presents the comparison for the plunging breaker case. In recognition of the more violent breaking associated with the plunging breaker, the eddy viscosity inside the surf-zone has been increased to $0.02h\sqrt{gh}$. The figure indicates that even for the plunging breaker case the quantitative comparison is still quite good though it is a little worse than the previous case. For the plunging breaker case we also find, by integrating the measurements over depth and using (10), that the non-dimensional volume flux (defined as $Q_w/(H^2\sqrt{gh}/h)$) is very different in the experiment by Nadaoka & Kondoh (0.065) and the experiment by Ting & Kirby (0.018). This difference is probably related to the very different

values of h/L in the two experiments (0.025 for Ting & Kirby and 0.068 for Nadaoka & Kondoh at the break point). The low value of h/L in the Ting & Kirby experiment causes the waves to have short peaky crests which gives a small value of $Q_w/(H^2\sqrt{gh}/h)$ (see, e.g., Cokelet 1977).

4 Discussion

As pointed out in the introduction, the main features to notice about the undertow outside the surf-zone are: 1) it has very little curvature and 2) the shape of the profile is quite different from what it is inside. The first of these is readily understood by comparing the forcing for the undertow inside and outside the surf-zone. Outside the surf-zone, the forcing is given by

$$\alpha_1 = \frac{-\tau_b}{\rho h} \sim \frac{f_w u_0 U_b}{h} \sim \frac{f_w}{2}\frac{H}{h}\frac{U_b}{c}g \tag{29}$$

which, for typical values of the parameters ($f_w = 0.02$, $U_b/c \leq 0.05$, $H/h \leq 0.6$), gives the following estimate for α_1

$$\alpha_1 \leq 3 \times 10^{-4} g \tag{30}$$

which is much smaller than the forcing for the undertow encountered inside the surf-zone (equation 20). Equation 12 shows that the forcing is directly proportional to the curvature and hence the very small forcing estimated by (30) leads to a very small curvature on the profile.

The results presented in the previous section indicate that accounting for the steady streaming brings the model results in line with the observations. This may be understood by considering that the steady streaming typically results in a velocity in the direction of wave propagation, which tends to reduce the near bottom velocity of the undertow. Since the total volume flux to be returned by the undertow is fixed, the slope of the undertow profile will at the same time be increased.

It is worthwhile to emphasize that the the steady streaming is not a fixed velocity. It basically is a response to the the Reynolds' stress (corresponding to the $\overline{u_w w_w}$ term)

generated by the boundary layer. Thus, the present results indicate that the actual effect that the Reynolds' stress has on the velocity profiles is radically different inside and outside the surf-zone.

Acknowledgements: We would like to thank F. C. K. Ting (Texas A & M University) and J. T. Kirby (University of Delaware) for making the experimental data of Ting & Kirby (1993) available for comparison before their publication. This work is a result of research sponsored by NOAA Office of Sea Grant, Department of Commerce, under Grant No. NA86AA-D-SG040 (Project No. R/OE 6). The U.S. Government is authorized to produce and distribute reprints for government purposes notwithstanding any copyright notation that may appear herein.

References

Cokelet, E. D., 1977. Steep gravity waves in water of arbitrary uniform depth. Philosophical Transactions of the Royal Society of London, 286, pp. 183-230.

Dally, W. R. and R. G. Dean, 1984. Suspended sediment transport and beach profile evaluation. Journal of Waterway, Port, Coastal and Ocean Engineering, ASCE, 110, pp. 15-33.

deVriend, H. J. and M. J. F. Stive, 1987. Quasi-3D modelling of nearshore currents. Coastal Engineering, 11, pp. 565-601.

Dyhr-Nielsen, M. and T. Sorensen, 1970. Some sand transport phenomena on coasts with bars. Proceedings of the 12th Coastal Engineering Conference, pp. 855-66.

Greenwood, B. and P. D. Osborne, 1990. Vertical and horizontal structure in cross-shore flows: An example of undertow and wave set-up on a barred beach. Coastal Engineering, 14, pp. 543-580.

Guza, R. T. and E. B. Thornton, 1985. Velocity moments in the nearshore. Journal of

Waterway, Port, Coastal and Ocean Engineering, ASCE, 111, pp. 235-256.

Hansen, J. B. and I. A. Svendsen, 1984. A theoretical and experimental study of the undertow. Proceedings of the 19th Coastal Engineering Conference, Houston. pp. 2246-2262.

Hansen, J. B. and I. A. Svendsen, 1986. Experimental investigation of the wave and current motion over a longshore bar. Proceedings of the 20th Coastal Engineering Conference, Taipei. pp. 1166-1179.

Hwung, H. H. and C. Lin, 1990. The mass transport of waves propagating on a sloping bottom. Proceedings of the 22nd Coastal Engineering Conference. pp. 544-556.

Mei, C. C. 1983. The applied dynamics of ocean surface waves. John Wiley and Sons, New York, 740 pp.

Nadaoka, K., and T. Kondoh, 1982, Laboratory measurements of velocity field structure in the surf zone by LDV. Coastal Engineering in Japan, 25, pp. 125-145.

Okayasu, A., T. Shibayama and K. Horikawa, 1988. Vertical variation of undertow in the surf-zone. Proceedings of the 21st Coastal Engineering Conference, pp. 478-491.

Okayasu, A., T. Shibayama and N. Mimura, 1986. Velocity field under plunging waves. Proceedings of the 20th Coastal Engineering Conference, pp. 660-674.

Phillips, O. M., 1977. The dynamics of the upper ocean. Cambridge University Press, 336 pp.

Stive, M. J. F. and H. J. deVriend, 1987. Quasi-3D nearshore current modelling: Wave induced secondary currents. Proceedings of a special conference on coastal hydrodynamics, ASCE, Newark, pp. 356-370.

Stive, M. J. F. and H. G. Wind, 1982. A study of radiation stress and set-up in the nearshore region. Coastal Engineering, 6, pp. 1-26.

Stive, M. J. F. and H. G. Wind, 1986. Cross-shore mean flow in the surf-zone. Coastal Engineering, 10, pp. 325-340.

Svendsen, I. A., 1984. Mass flux and undertow in a surf-zone. Coastal Engineering, 8, pp. 347-365.

Svendsen, I. A. and J. B. Hansen, 1986. Interaction of waves and currents over a longshore bar. Proc. 20th Coastal Engineering Conference, pp. 1580-1594.

Svendsen, I. A. and J. B. Hansen, 1988. Cross-shore currents in surf-zone modelling. Coastal Engineering, 12, pp. 23-42.

Svendsen, I. A. and R. S. Lorenz, 1989. Velocities in combined undertow and longshore currents. Coastal Engineering, 13, pp. 55-79.

Svendsen, I. A. and Putrevu, U. 1993. Nearshore mixing and dispersion. Submitted for publication.

Svendsen, I. A., H. A. Schaffer and J. B. Hansen, 1987. The interaction between the undertow and boundary layer flow on a beach. Journal of Geophysical Research 92, pp. 11,845-856.

Ting, F. C. K. and J. T. Kirby, 1993. Observation of undertow and turbulence in a laboratory surf-zone. In preparation.

Wright, L. D., R. T. Guza and A. D. Short, 1982. Dynamics of a high energy dissipative surf-zone. Marine Geology, 45, pp. 41-62.

List of figures

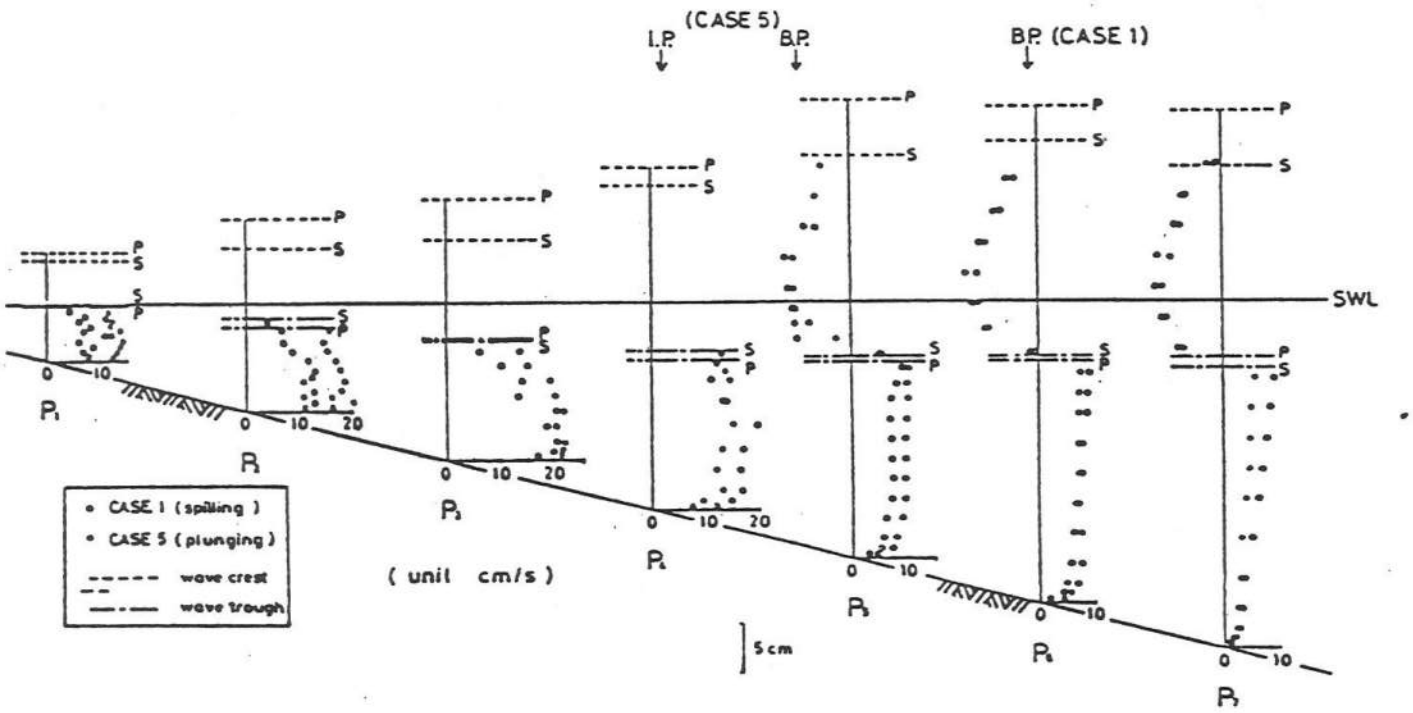
(CASE 5)
I.P.
B.P.
B.P. (CASE 1)
SWL
P
S
0
10
20
P1
P2
P3
P4
P5
P6
• CASE 1 (spilling)
• CASE 5 (plunging)
wave crest
wave trough
(unit cm/s)
5cm

FIGURE 1

FIGURE 2

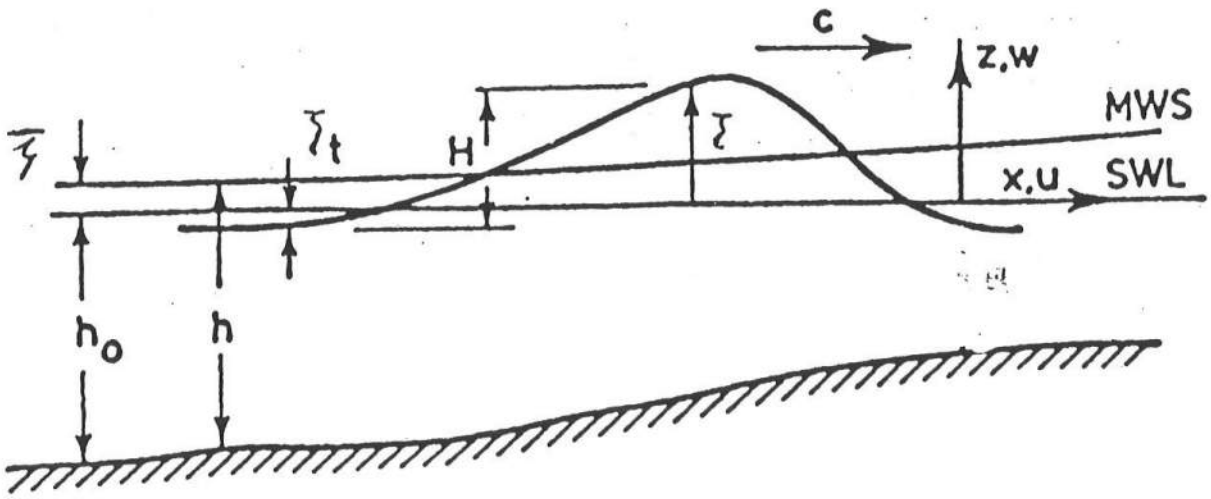

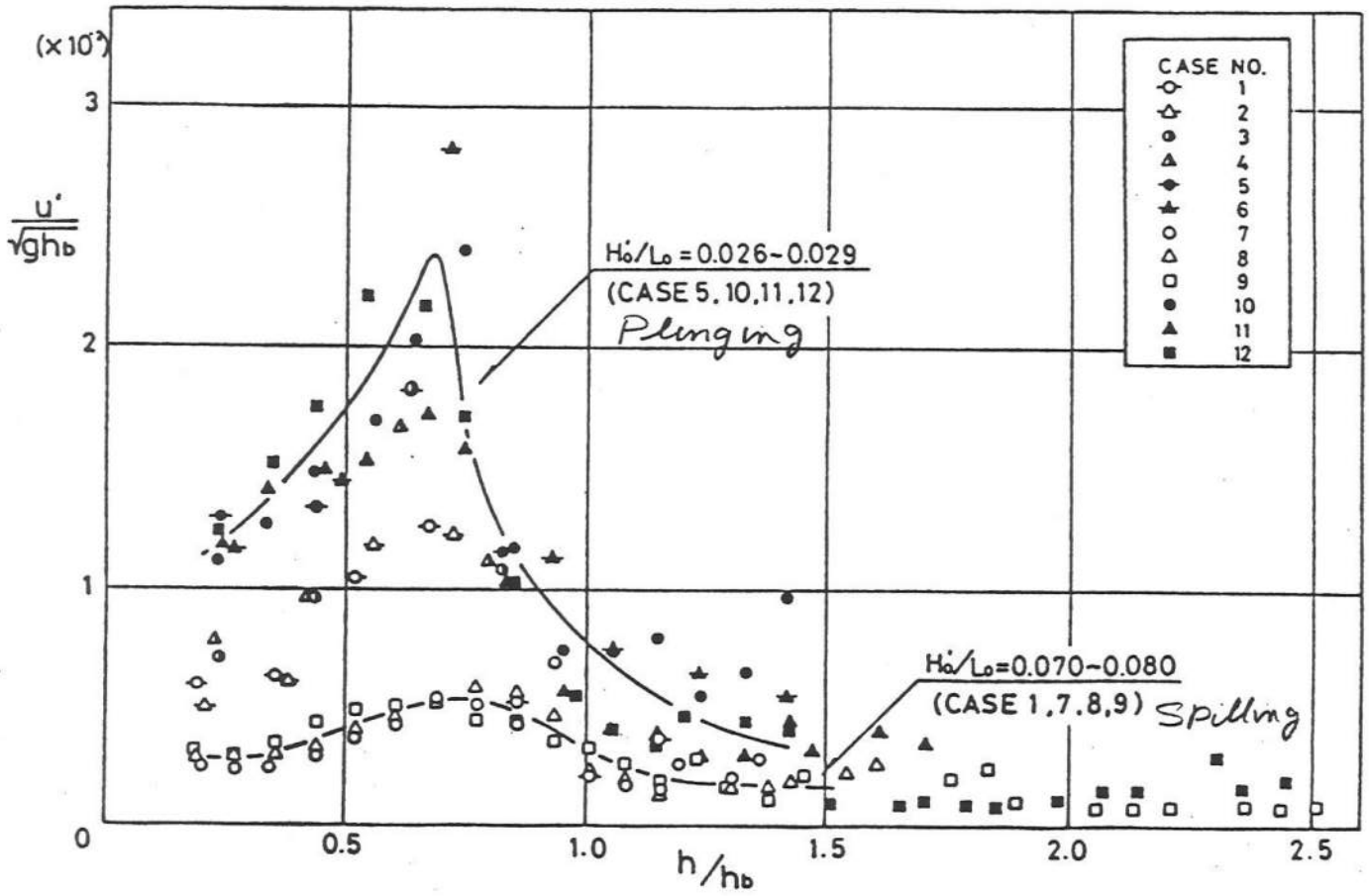
(×10⁻²)
3
2
1
0
u'/√ghb
0.5
1.0
1.5
2.0
2.5
h/hb
CASE NO.
1
2
3
4
5
6
7
8
9
10
11
12
Hb/Lo = 0.026~0.029
(CASE 5, 10, 11, 12)
Plunging
Hb/Lo=0.070~0.080
(CASE 1, 7, 8, 9) Spilling

FIGURE 3

Figure 4

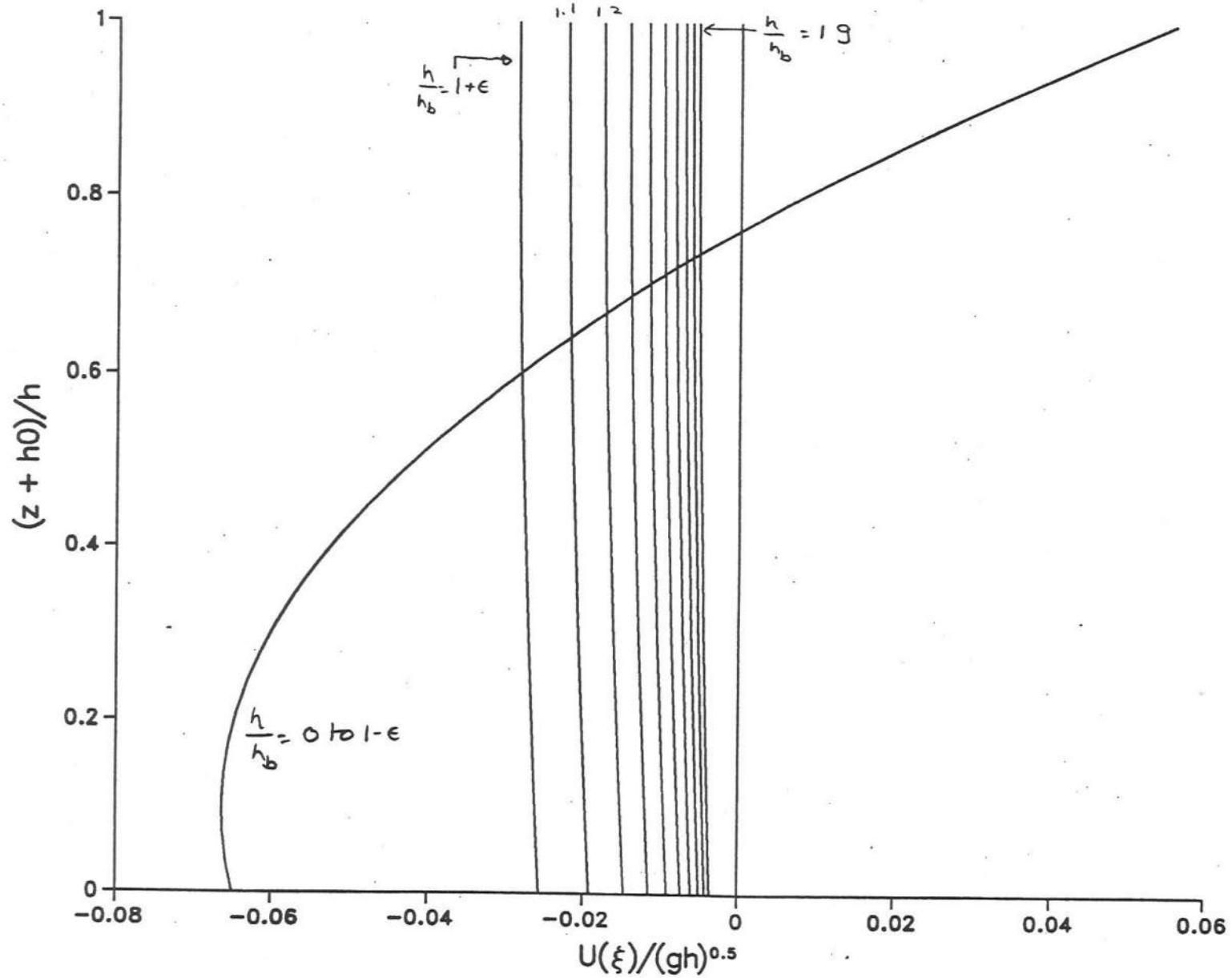
1.1
1.2
h/hb = 1.9
h/hb = 1+ε
h/hb = 0 to 1-ε
1
0.8
0.6
0.4
0.2
0
−0.08
−0.06
−0.04
−0.02
0
0.02
0.04
0.06
(z + h0)/h
U(ξ)/(gh)^0.5

Figure 5

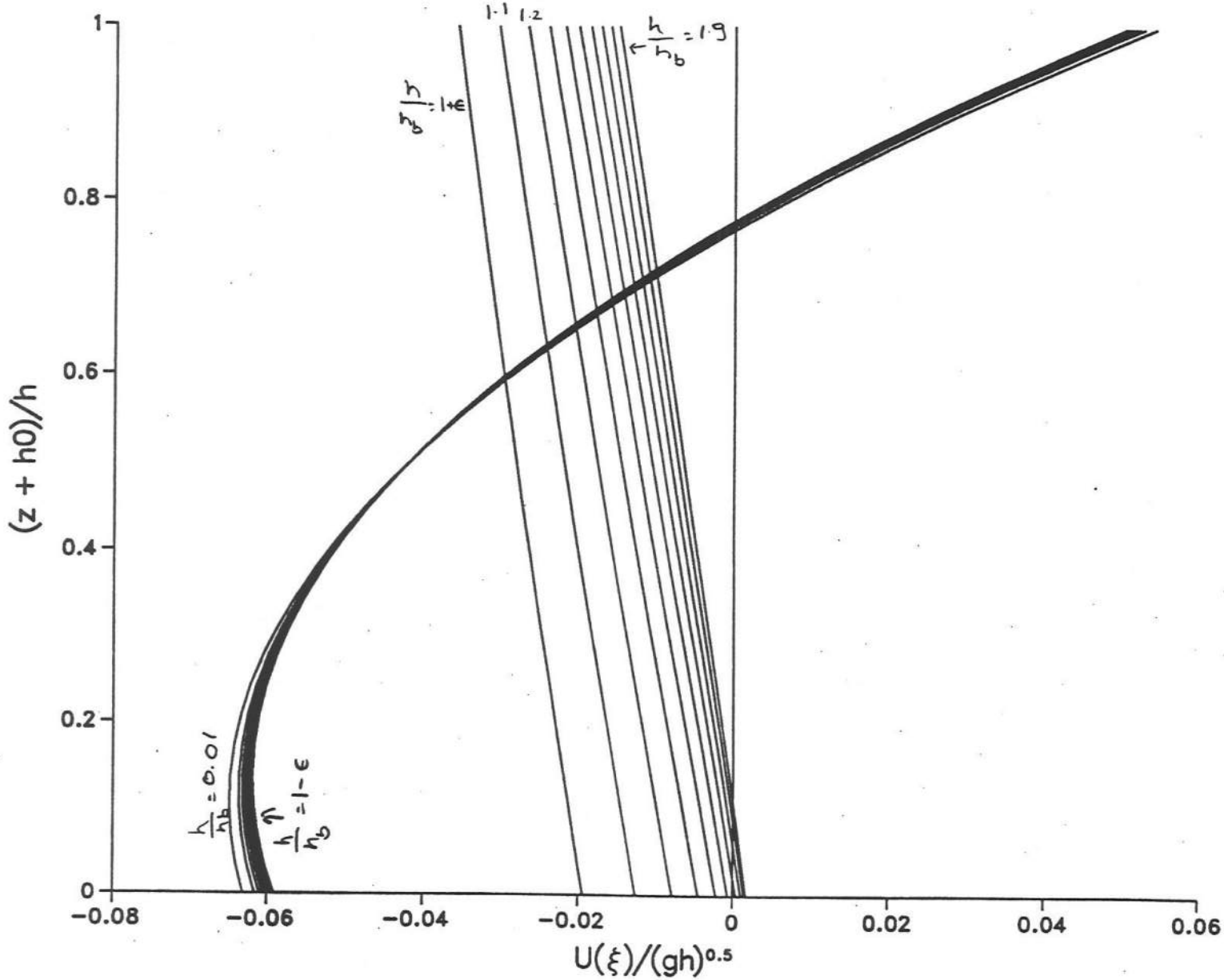
1
0.8
0.6
0.4
0.2
0
(z + h0)/h
−0.08
−0.06
−0.04
−0.02
0
0.02
0.04
0.06
U(ξ)/(gh)^0.5
1.1
1.2
h/hb = 1.9
h/hb = 1+ε
h/hb = 0.01
h/hb = 1−ε

Figure 6

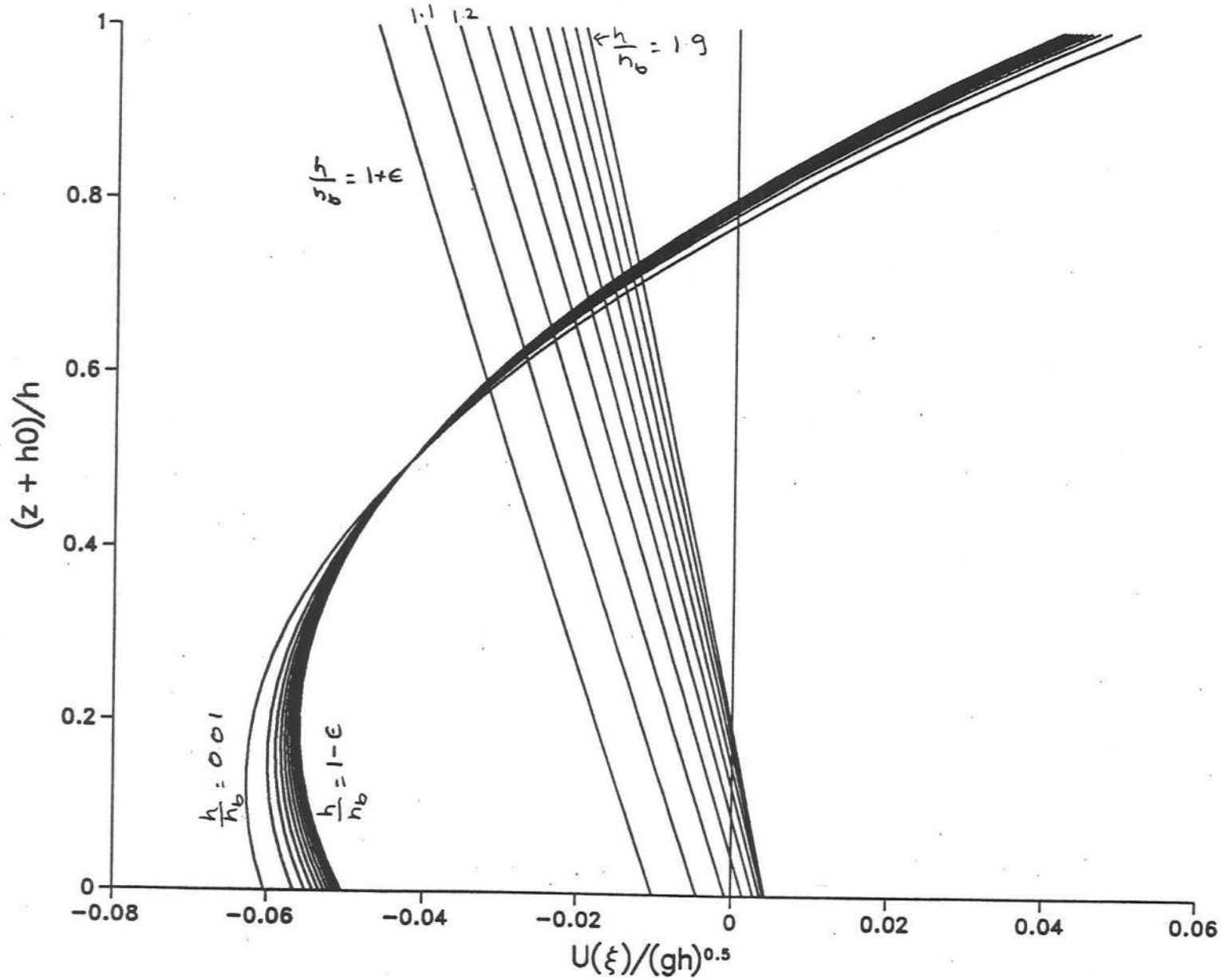
1.1
1.2
$\frac{h}{h_b} = 1.9$
$\frac{h}{h_b} = 1+\epsilon$
$\frac{h}{h_b} = 0.01$
$\frac{h}{h_b} = 1-\epsilon$
(z + h0)/h
$U(\xi)/(gh)^{0.5}$
1
0.8
0.6
0.4
0.2
0
−0.08
−0.06
−0.04
−0.02
0
0.02
0.04
0.06

Figure 7

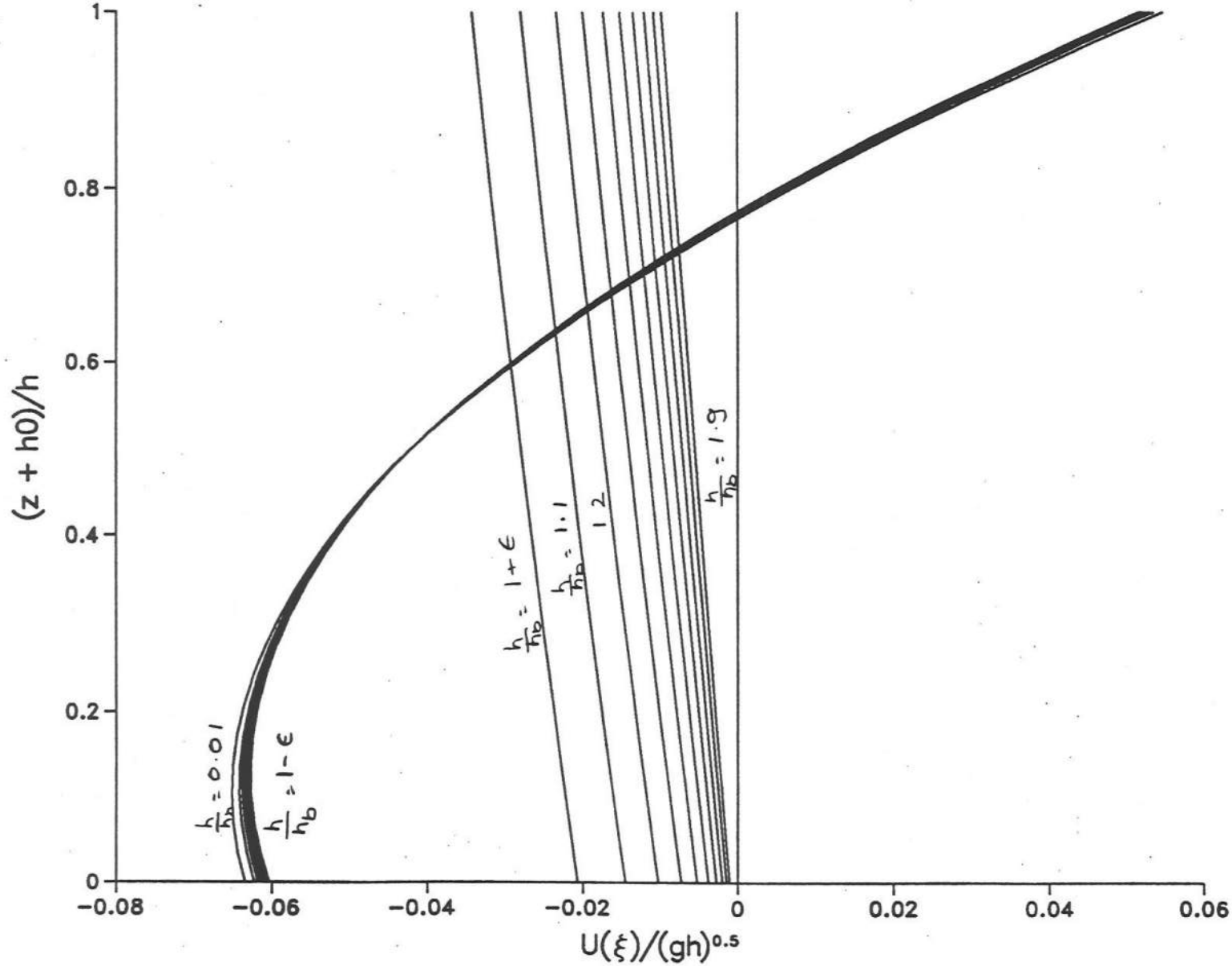
1
0.8
0.6
0.4
0.2
0
(z + h0)/h
−0.08
−0.06
−0.04
−0.02
0
0.02
0.04
0.06
U(ξ)/(gh)^0.5
h/hb = 0.01
h/hb = 1 − ε
h/hb = 1 + ε
h/hb = 1.1
1.2
h/hb = 1.9

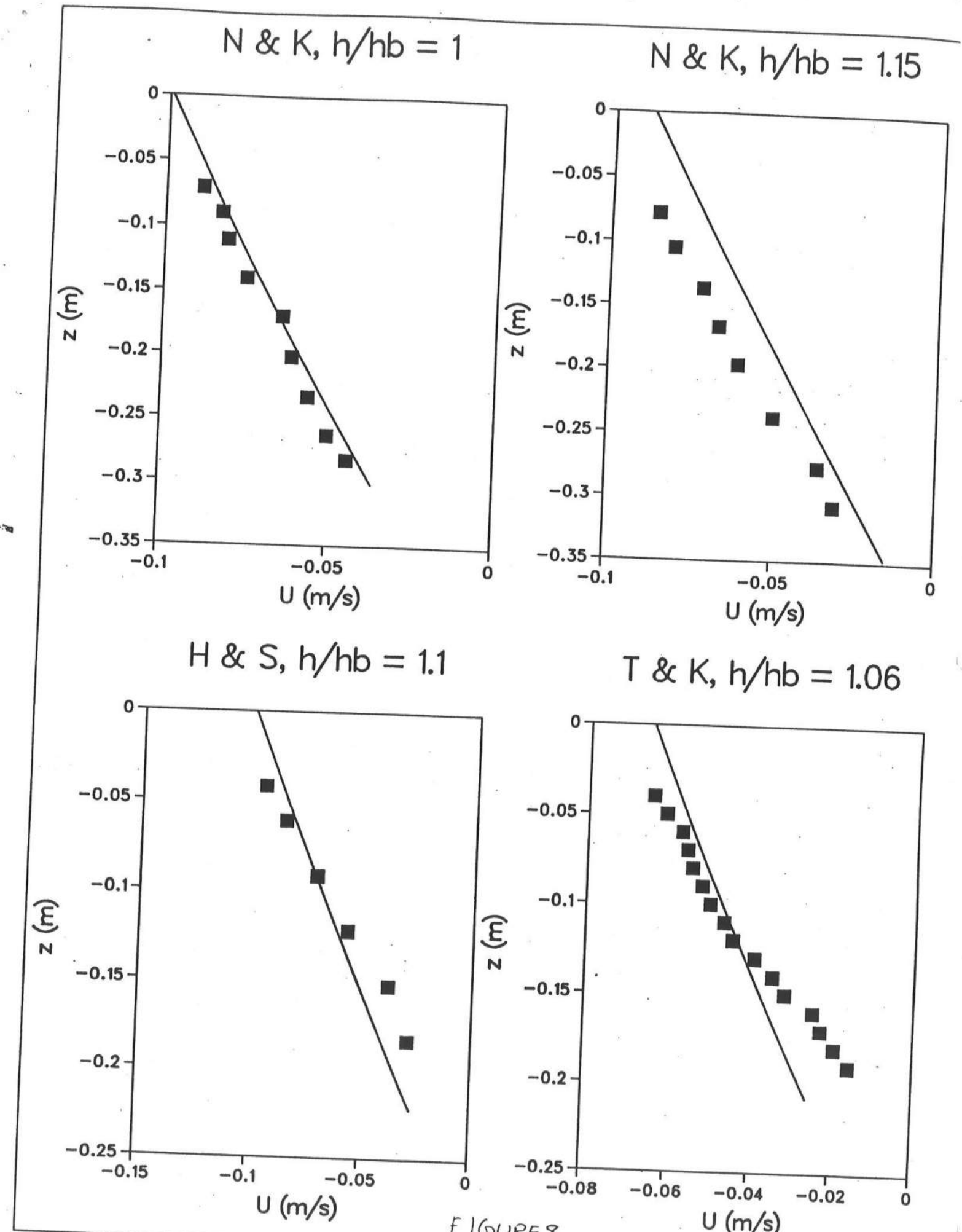
N & K, h/hb = 1
N & K, h/hb = 1.15
H & S, h/hb = 1.1
T & K, h/hb = 1.06
z (m)
U (m/s)
0
-0.05
-0.1
-0.15
-0.2
-0.25
-0.3
-0.35
-0.08
-0.06
-0.04
-0.02

FIGURE 8

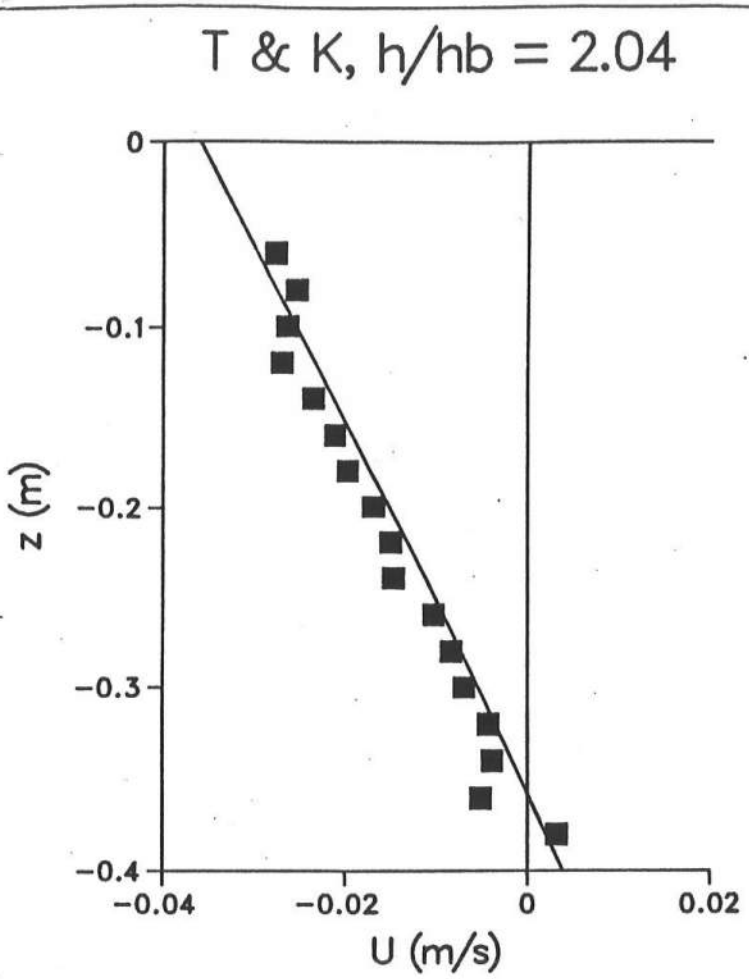

FIGURE 8 - Contd.

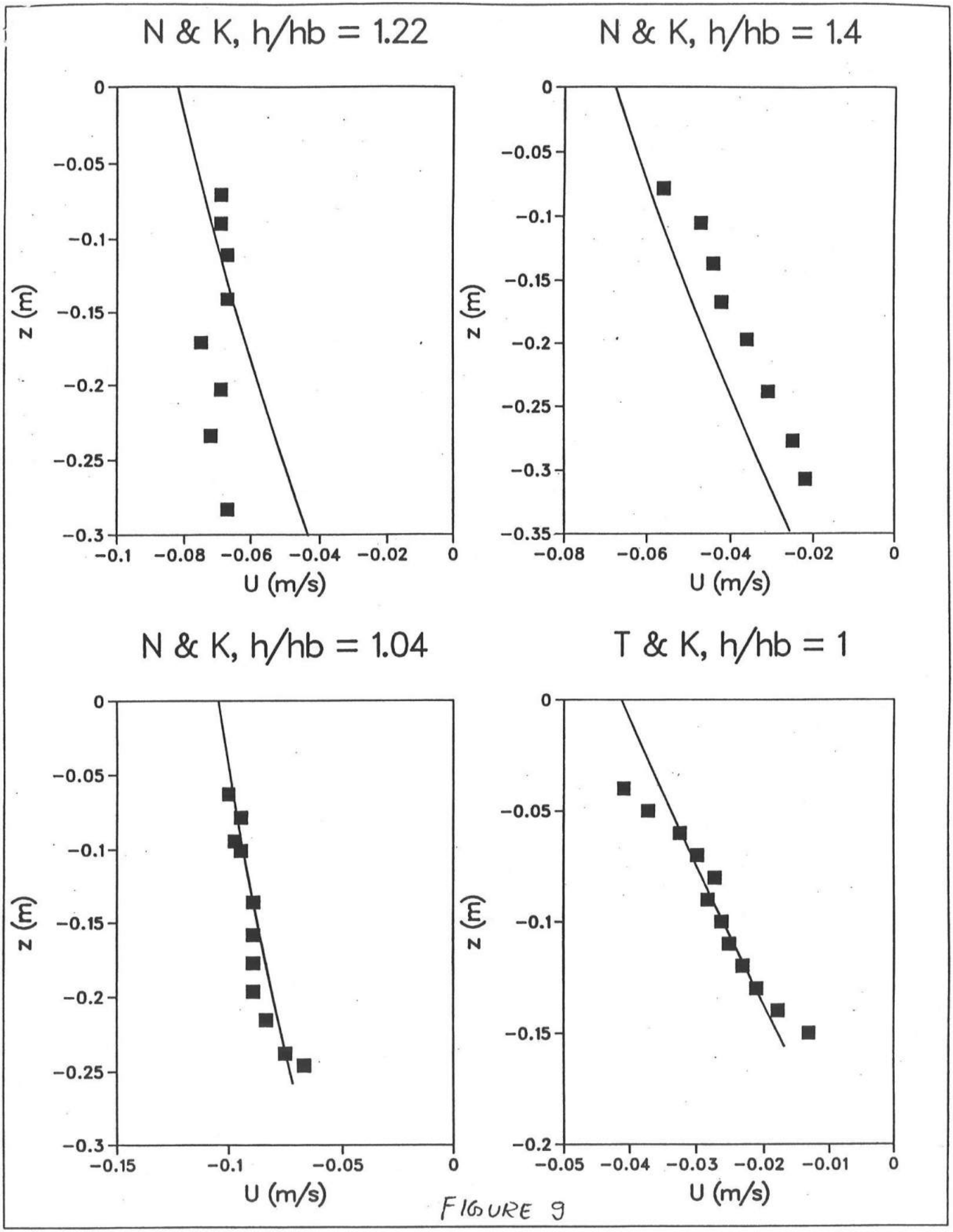
N & K, h/hb = 1.22
N & K, h/hb = 1.4
N & K, h/hb = 1.04
T & K, h/hb = 1
z (m)
U (m/s)
0
-0.05
-0.1
-0.15
-0.2
-0.25
-0.3
-0.35
-0.1
-0.08
-0.06
-0.04
-0.02
-0.15
-0.05
-0.03
-0.01

FIGURE 9

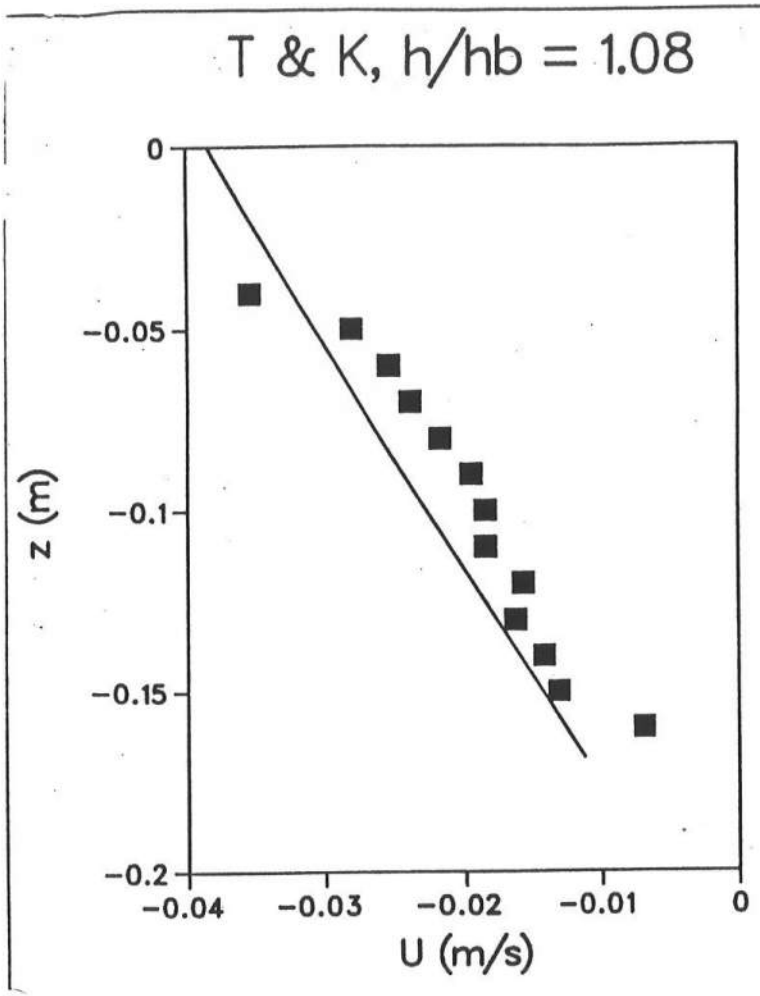

FIGURE 9 - Contd.